Sub-wavelength Focusing and Imaging Using Shifted-beam and Super-oscillation Antenna Arrays

George V. Eleftheriades, Loïc Markley and Alex M. H. Wong

Department of Electrical and Computer Engineering
University of Toronto
Canada
gelefth@waves.utoronto.ca

We review our recent research on the development of structures that can focus electromagnetic waves down to sub-wavelength spots for detection and imaging applications. Emphasis is placed on increasing the "working distance" from the focusing apparatus. For this purpose, we have developed optimized near-field antennas arrays ("meta-screens") that are designed using the notion of the "shifted beams". We have also developed super-oscillation antenna arrays that do not utilize evanescent waves and thus can increase the working distance at the multi-wavelength range. Example applications in imaging and detecting buried objects as well as in super-resolving radars are presented.

Keywords: antenna arrays, super-resolution, evanescent waves, near field, imaging, super-oscillations, radars.

I. INTRODUCTION

We review our recent research on the development of structures that can focus electromagnetic waves down to sub-wavelength spots for detection and imaging applications. A great challenge is to achieve this kind of focusing over an appreciable "working distance" from the focusing apparatus. For this purpose, we have developed antenna structures ("meta-screens") that are designed using the notion of the "shifted beams" [1]. We have developed suitable near-field antenna arrays to implement this concept and we are describing corresponding sub-wavelength imaging experiments in free space as well as for buried objects. These near-field antenna arrays utilize evanescent waves to increase the resolution and therefore the corresponding imaging range is limited in practice to distances less than half a wavelength. Nevertheless, meta-screens are attractive since they are easy to fabricate, are scalable from microwave to optical wavelengths and the focusing is insensitive to material losses.

In order to extend the "working distance" even further, we have also experimented with the concept of the super-oscillation which does not use evanescent waves. We have shown that the classical antenna super-directivity by Schelkunoff is a super-oscillation phenomenon in the spectral domain [2]. Based on this approach, we have designed and experimentally demonstrated simple antenna arrays that can produce local sub-wavelength spots at multi-wavelength working distances in a waveguide environment. Recent radar range super-resolution experiments are also described.

II. SHIFTED-BEAM THEORY

Shifted beam theory was developed as a tool for designing near-field antenna arrays [1]. Applications in areas like near-field focusing and near-field imaging require evanescent field manipulation and such arrays cannot be designed using classical far-field antenna array theory. Shifted-beam theory is a near-field array theory based on the observation that the concept of an array factor doesn't exist in the near-field of an antenna array. In the far-field, the displacement of an antenna element from the origin results in a phase shift being applied to the field pattern. In the near-field however, the entire field pattern is displaced along with the element, resulting in changes to both the phase and magnitude of the field pattern. Equation (1) states this distinction mathematically.

$$E_{shifted}(x) = \begin{cases} E_0(x)e^{-jkx_0 \sin\theta\cos\phi} & \text{far field} \\ E_0(x - x_0) & \text{near field} \end{cases} \tag{1}$$

The nature of the element patterns in the near-field and the far-field is illustrated in Fig. 1. We can see that the near-field patterns are spatially shifted from one another, providing a linear independence that can be exploited to synthesize near-field patterns.

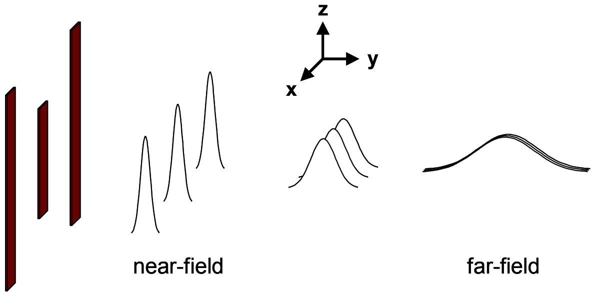

Figure 1. An illustration of the nature of array element field patterns in the near-field and in the far-field.

The total field at some distance $y = h$ can be written as in (2) where *f(x)* is the target field distribution and $E_n(x)$ are the element field patterns. This can be recognized as a

978-1-4673-0292-0/12/$31.00 ©2012 IEEE

method-of-moments type of a problem, from which the optimal weights w_n can be determined.

$$E_{tot}\left(x,h\right)=\sum_{n=1}^{N} w_n E_n\left(x,h\right)\approx f\left(x\right) \qquad (2)$$

If we discretize the fields over a set of points x_k such that $\mathbf{f}[k]=f(x_k)$ and $\mathbf{A}[k]=[\mathbf{E}_1[k] \;\; \cdots \;\; \mathbf{E}_N[k]]$ and use the element field patterns as weighting functions, the optimal weights can be calculated using (3).

$$\mathbf{w}_{opt}=\left(\mathbf{A}^H\mathbf{A}\right)^{-1}\mathbf{A}^H\mathbf{f} \qquad (3)$$

The optimized weights can be translated into a physical geometry through a detailed calculation of the array impedance matrix. Using well known self and mutual impedance equations with a length compensation factor to reduce the discrepancy between the assumed dipole current distribution and the actual distribution, the full $\boldsymbol{Z}$ matrix can be computed. In the case of a centrally fed dipole, the applied voltage is zero everywhere but at the central element, and the currents can be determined using $\mathbf{I}=\mathbf{Z}^{-1}\mathbf{V}$. By changing the dimensions of the antenna elements, the current ratios can be quickly calculated and compared to the optimal shifted beam weights until a match is found.

III. END-FIRE ARRAY PROBE FOR BURIED OBJECTS

A near-field focusing array was designed using shifted beam theory to produce a focal spot inside a dielectric material at a distance a quarter-wavelength. The array was designed to operate as a near-field scanning probe to detect objects buried within the dielectric. In this scenario the distance from the probe to the objects is constrained by the dielectric and the working distance cannot be reduced [3],[4].

The array was fed directly through a coaxial line connected to the central element. The satellite elements were excited parasitically. By tuning the lengths of the elements, the impedance matrix of the array could be tuned so that the element currents were out-of-phase and their ratio matched the optimal weights determined by the shifted beam algorithm.

The antenna array was used as a probe by monitoring the input reflection coefficient for perturbations as it was raster scanned over the surface of a sample under test. The presence of small objects of strong permittivity would disturb the near-field surrounding the probe, thereby changing its input impedance. A detection signal was acquired by renormalizing the input impedance using (4), where Γ_0 was the input impedance in the absence of any object, and normalizing with respect to the peak value.

$$\hat{\Gamma}=\frac{\Gamma-\Gamma_0}{1-\Gamma\Gamma_0} \qquad (4)$$

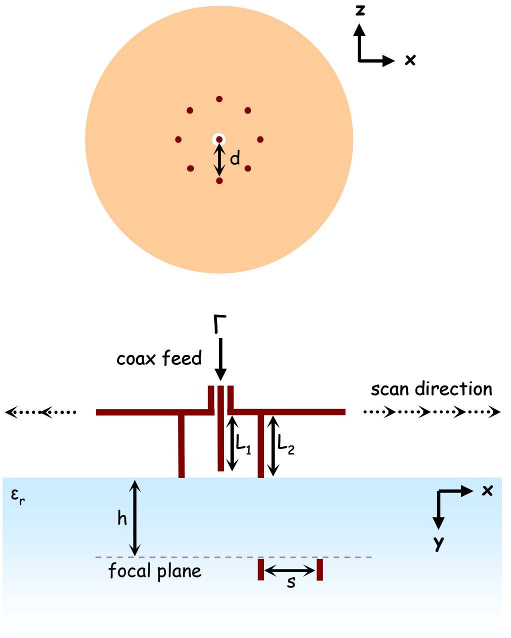

Figure 2. An illustration of the end-fire array probe and the scanning method using for imaging objects buried within a dielectric.

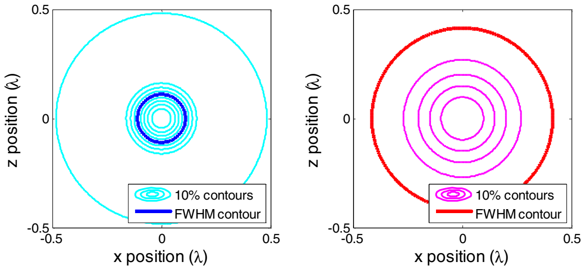

Figure 3. Focal plane contour plots of the longitudinal electric field for the array probe (blue, left) and the single monopole probe (red, right). The FWHM contour is highlighted using a thicker line.

The final array geometry was designed to operate at a frequency of 2.4 GHz ($\lambda_0 = 125\,\text{mm}$) with $d = 0.15\lambda_0$ (12.9 mm), $L_1 = 0.218\lambda_0$ (27.2 mm), and $L_2 = 0.256\lambda_0$ (32.0 mm), using dipoles of width $a = 0.01\lambda_0$ (1.25 mm). The array was designed to produce a confined focal spot within the dielectric where the wavelength was $\lambda = 86.3\,\text{mm}$. Figure 3 plots the longitudinal electric field E_y at the focal plane for this geometry in the left figure with blue contours. The data was simulated using FEKO, a full-wave electromagnetics method-of-moments numerical tool. The focused field has a full-width half-maximum (FWHM) beam width of 0.220λ (dielectric wavelengths) with side levels under 20%. The figure on the right with red contours shows the focal plane for a single monopole antenna as a comparison. The FWHM beam width for the single monopole field is 0.829λ.

The probe was fabricated by attaching a semi-rigid coax line to a copper ground plane and allowing the inner conductor to penetrate through to the other side, forming the central element. Eight bare wires were then soldered around the central element, forming the satellite antennas. The probe was connected to an Agilent E8364B network analyzer and held in a fixed position while a container filled with mineral oil was placed above. The mineral oil provided a low-loss dielectric with relative permittivity 2.1. Two short dipole objects were suspended in the fluid using a PTFE support structure and scanned across the probe using a custom build XYZ translator from Newmark Systems. The object spacing could be adjusted to fully characterize the probe resolution. The entire experimental domain was surrounded in ECCOSORB AN-77 absorbing material to reduce reflections. A photograph of the apparatus is shown in Fig. 4.

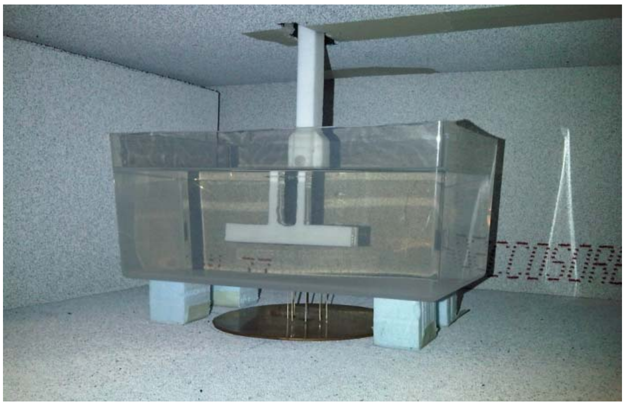

Figure 4. A photograph of the experimental apparatus. A container filled with mineral oil provided the dielectric in which two dipole objects were positioned. The probe was placed facing up underneath the container to measure the perturbations in the field due to the presence of the objects.

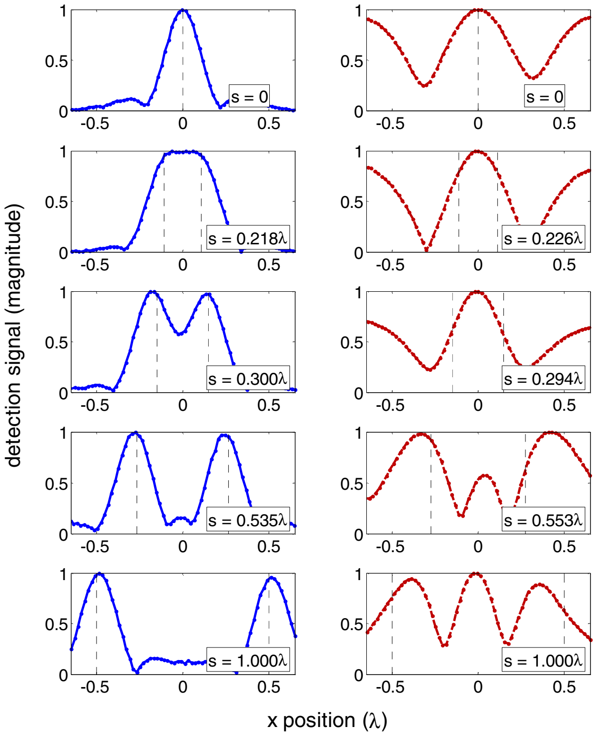

Figure 5. Experimentally measured detection signals of one and two objects separated by various distances *s*. The blue traces (left column) are from the array probe while the red traces (right column) are from the single monopole probe. The actual object locations are indicated by the vertical dashed lines.

The measured detection signals are plotted in Fig. 5 for the array probe (blue, left column) and the single monopole probe (red, right column). The single object signals (in the width of 0.231λ and 0.446λ, respectively, although the side levels are much worse for the single monopole top row) show a FWHM beam signal.

These results were interpolated to find the minimum resolvable separation (defined as the point where the dip between detection beak fell below 71%). For the array probe this was at 0.279λ ($0.190\lambda_0$) while for the monopole probe it was at 0.504λ ($0.343\lambda_0$). Although this seems to indicate only twice the resolution enhancement, we can see from Fig. 5 that the single monopole probe signal suffered from side lobe interference that resulted in false positives and poor object localization, even at separation distances as large as one wavelength (see the lower right plot in Fig. 5).

IV. SUPER-OSCILLATORY SUB-WAVELENGTH IMAGING

A. *Introduction*

The last few years saw the proposal of a new approach: to perform sub-wavelength imaging with *super-oscillatory* propagating waves. Super-oscillation is a phenomenon whereby a waveform oscillates faster than its highest constituent frequency component across a finite interval [5]. With the local availability of wave components which oscillate faster than traditionally thought to be possible, one can form a sharper focus with electromagnetic waves, and construct images with sub-wavelength resolution. Moreover, since only propagating waves are employed, super-oscillatory waves are not restricted by evanescent wave decay, and can thus bring sub-wavelength electromagnetic imaging capabilities to the far-field.

In the last five years, a few super-oscillatory focusing devices [6],[7] have been proposed, which prove that one can use super-oscillations to overcome traditional limits on device working distance. However, for these devices to be of widespread usage in everyday imaging applications, further work is needed to a) generate a super-oscillatory waveform in a deterministic, rather than probabilistic, fashion; b) better control the waveform characteristic both inside and outside the interval where super-oscillations occur; and c) construct devices which are robust against minor fluctuations, thus making them applicable in practical imaging environments.

B. *Super-oscillation and Super-directivity*

To achieve the aforementioned objectives to super-oscillatory sub-wavelength imaging, we proposed to view super-oscillation from a new perspective – from its relation to the phenomenon of super-directivity. Super-oscillation and super-directivity were similar in a key manner: the former allowed sub-diffraction spatial localization for waveforms of limited spectral extent (the spectral region of propagating waves); the latter allowed sub-diffraction angular beam widths for waveforms of limited spatial extent (the size of the antenna array). Our investigation showed that super-oscillation and super-directivity were dual phenomena, and one led to the other upon reversing the spatial and spatial frequency domains [2]. This new understanding on super-oscillation allowed us to leverage existing antenna design methods to design super-oscillatory waveforms. These design methods provided practical handles on key waveform parameters such as the focal width, the extent of the super-oscillatory region, and sidelobe levels within and without the super-oscillatory region. We have hence paved way for the practical design of super-oscillatory waveforms in imaging systems.

C. Super-oscillatory Waveform Design

We overview our design formulation for super-oscillatory waveforms, and refer interested readers to [2]. First we represented periodic image waveform $E_{img}(x)$ and its spectrum $\tilde{E}_{img}(k_x)$ as follows:

$$E_{img}(x) = Ca_{N-1}\prod_{n=1}^{N-1}(z-z_n) = C\sum_{n=0}^{N-1}a_n z^n\ ,$$
$$\text{where } z = e^{-jx\Delta k}\ ,\ C = e^{-jx\Delta k_{x0}} \tag{5}$$

$$\tilde{E}_{img}(k_x) = \sum_{n=0}^{N-1}a_n\delta(k_x - n\Delta k - k_{x0})\ . \tag{6}$$

Here a_n is the weighting of the n'th delta function, N is the number of plane waves – or number of delta functions in the spectral domain, Δk is the spacing between delta functions in the spectral domain, k_{x0} is the transverse frequency of the first (most negative) delta function and C is a phase constant which simplifies the notation in (6). Note that (5) resembles an antenna array factor. Hence, using Shelkunoff's methodology for antenna design, we chose the coefficients a_n to achieve desired super-oscillatory characteristics for the waveform $E_{img}(x)$. Subsequently, $\tilde{E}_{img}(k_x)$ was back-propagated from the image plane to the source plane, where antenna arrays are located. When the resultant source spectrum $\tilde{E}_{src}(k_x)$ was synthesized, the corresponding super-oscillatory waveform $E_{img}(x)$ would result at the predesigned image distance away from the screen.

Using this formulation, we designed an image waveform with a sub-wavelength central peak width, along with constant sidelobes at 20% peak field strength (4% intensity) for a region of λ/2 on both sides of the peak. Fig. 6 shows the results for this design. Fig. 6a shows zero locations on the complex z-plane. Fig. 6b shows the spectrum $\tilde{E}_{img}(k_x)$. Fig. 6c shows a half-period of the super-oscillatory waveform $E_{img}(x)$ (the other half-period had the same amplitude, but was π-shifted in phase). Fig. 6d displays a close-up of the waveform, and shows clear improvement compared to the diffraction-limited sinc function.

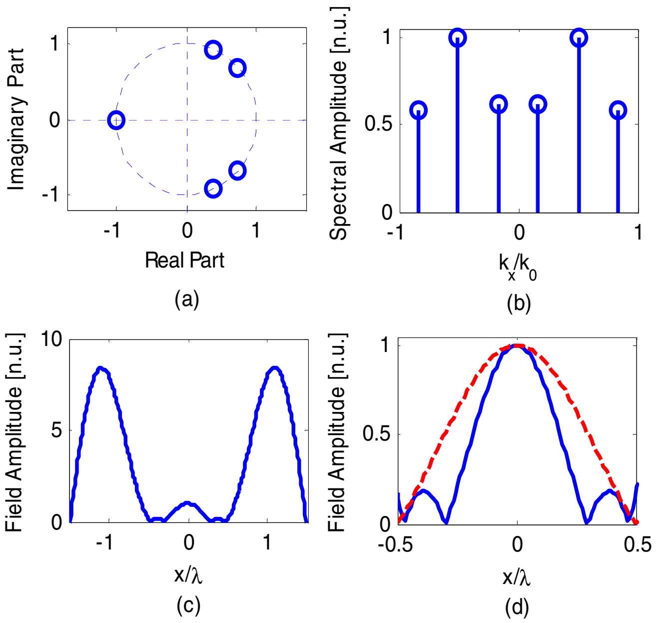

Figure 6. An example design of a super-oscillation pulse. (a) Zero locations in the Schelkunoff antenna design procedure. (b) Corresponding spectral diagram, showing clearly that only propagating wave components ($k_x < k_0$) are included. (c) A half period of the super-oscillation waveform. (d) A close up of the super-oscillatory region, showing a sharpened peak compared to the diffraction-limited sinc function (red dashed line).

D. Antenna Array for Sub-wavelength Focusing within a Waveguide

We synthesized the above-designed waveform in a waveguide environment [8], which is schematically shown in Fig. 7. We used a rectangular waveguide with cross-sectional dimensions 297mm by 13mm. At the source plane, 10 co-axial ports provided inputs and outputs to five line-sources, which were spaced λ/2 (50mm) apart and embedded within the rectangular waveguide. Driving these line-sources through a tunable feeding network, we excited the TE10, TE30 and TE50 waveguide modes in appropriate proportion, such that after five wavelengths (500mm) of propagation within the waveguide, their spectral relation would become that shown in Fig. 6b, and hence their superposition would result in the sub-wavelength super-oscillatory focus shown in Fig. 6c. A coaxial probe was scanned across a series of image planes around 500mm away from the source plane to measure the electric field along the direction of the line-sources. Fig. 8 plots the measured electric field (blue) within the super-oscillatory design region of a cross-section 480mm away from the screen plane. Comparison with the focal field obtained from a full wave simulation using Ansoft HFSS (red, dashes) showed good simulation-experiment agreement. The focusing capability had been slightly compromised compared to the designed waveform shown in Fig. 6, due mainly to the imperfect termination at the waveguide end facet where the coaxial probe was inserted. Notwithstanding, the experimentally obtained focus had an electric field FWHM of 45mm (0.45λ), which was 75% of the width of a diffraction-limited waveform, obtained from the in-phase superposition of equal proportion of all three waveguide modes. Hence in this experiment we conclusively

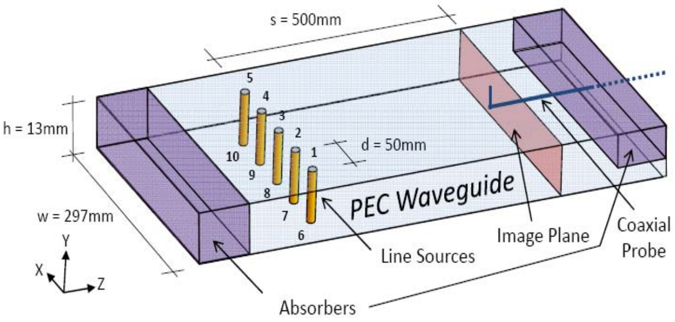

Figure 7. A schematic of the experimental setup, showing waveguide dimensions, source and image plane locations, waveguide terminations and the configuration for the coaxial probe.

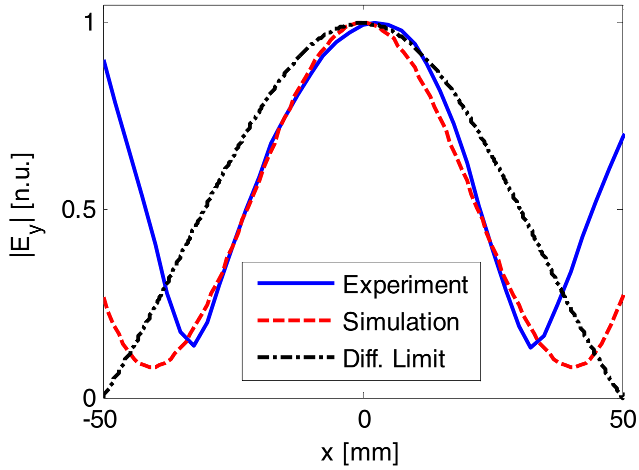

Figure 8. A plot showing the super-oscillatory region of the imaged electric field. Comparing the experimental and simulated super-oscillatory foci across the design interval. The diffraction-limited focus in this waveguide environment is also included for comparison.

demonstrated sub-wavelength microwave focusing at a multi-wavelength image distance. Scanning this sub-wavelength focus across a sample and measuring the scattered radiation would enable one to perform sub-wavelength imaging at this distance.

V. TEMPORAL SUPER-OSCILLATION SIGNALS

The design formulation we developed in the previous section can also be applied to generate temporal super-oscillatory waveforms, and thus produce arbitrarily sharp temporal pulses within a fixed bandwidth [9]. For this purpose, we designed a temporal super-oscillatory pulse through a procedure similar to Section IV. C. We then used this pulse as the imaging pulse in a radar system [10]. An object's range (distance from antenna) is given by

$$d = \frac{c_0 \tau}{2} \pm \frac{R_{3dB}}{2}, \tag{7}$$

where d is the radar range, c_0 is the speed of light in free-space, τ is the temporal delay accrued by the reflected signal, and R_{3dB} is the 3dB range resolution. Since (7) maps the radar range linearly to the temporal delay, we expected a super-oscillatory pulse with narrowed temporal width would improve the range resolution of a radar system beyond fundamental bandwidth limitations.

Our radar system operated as follows. First we used the 500MHz radar pulse to modulate a 4.2GHz carrier. After this, we sent the signal through a horn antenna, and with the same antenna we received the back reflection signal from a scattering target (a metallic plate). Finally we demodulated and observed the signal on an oscilloscope. Calibration with one known distance allowed us to determine the range of the metallic plate. Fig. 9 shows the improvement in range resolution obtained when the aforementioned super-oscillatory pulse was used to detect a scatterer nominally 3.45m away from the antenna. Using the super-oscillatory pulse, the 3dB range resolution was reduced by 36% – from 12.0cm for the sinc pulse to 7.7cm for the super-oscillatory pulse.

We proceeded to investigate the super-oscillatory pulse's capability to resolve two targets which only slightly differed in their radar ranges. Our calculations showed that our designed super-oscillatory radar pulse could resolve two scatterers separated by distances ranging from 12cm to 18cm, whereas the transform-limited sinc pulse failed to do so. Preliminary experimental results confirmed this finding. The top plot of Fig. 10 shows the reflection trace for the super-oscillatory pulse when we modified our experiment to use two scatterers placed 14cm apart (in the longitudinal sense). Two peaks were clearly resolved, with the peak separation of 17.3cm, which was within the error bounds of the 14cm separation. The two scatterers could not be resolved using the sinc pulse (Fig. 10b, bottom); instead, the corresponding reflection trace contained a single peak located near the average range of the two distinct scatterers.

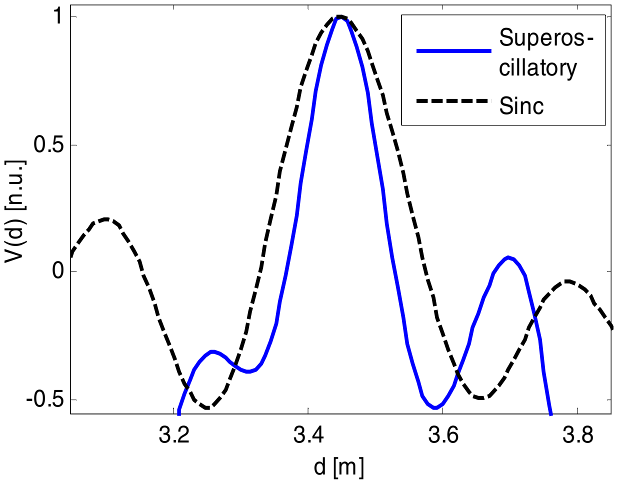

Figure 9. Comparison on range resolution at d=3.45m. The 3dB resolution for the super-oscillatory pulse is 7.7 cm. This resolution is 36% improved from the measured 3dB width of 12.0 cm for a 500 MHz sinc pulse reflected from the same distance.

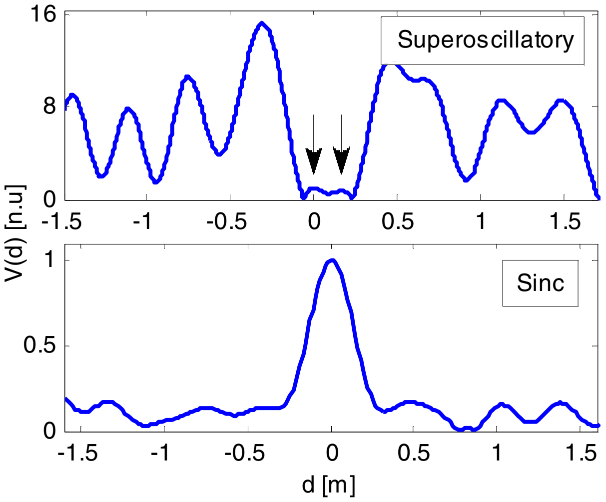

Figure 10. The measured reflection signal from the two target resolution radar experiment. The top plot shows that super-oscillation radar pulse resolving the two targets to be 17.3cm apart. Whereas the true separation is 14cm – within the error bounds given the width of the super-oscillatory waveform. The more pronounced peaks are high-energy oscillations which lie beyond the super-oscillatory region. The bottom plot shows that the scatterers cannot be resolved with a sinc radar pulse of the same bandwidth.

VI. CONCLUSION

In this paper we have described several structures that produce sub-wavelength focal spots outside the extreme near-field. A near-field antenna array theory called shifted beam theory is described and used to design an end-fire antenna array probe that can detect buried objects with sub-wavelength resolution. After conducting an experiment using two objects submersed in mineral oil at a working distance of 0.25λ, the minimum object separation which can be resolved by the array probe was determined to be 0.279λ ($0.190\lambda_0$). We have also described a waveguide-embedded super-oscillatory antenna array, whereby using only propagating waves, we demonstrated the forming of a sub-wavelength electromagnetic focal spot of 0.45λ, at five wavelengths away from the antenna array. This proves one can perform practical sub-wavelength imaging with working distance unconstrained by the evanescent near-field. Finally, we showed that one can use the theory of super-oscillations to improve the range resolution in radar systems. We experimentally demonstrated that a 500MHz temporal super-oscillatory pulse detected a single object with 36%-improved range precision, and resolved two closely spaced objects which were not resolvable by the 500MHz sinc pulse.

REFERENCES

[1] L. Markley, A.M.H. Wong, Y. Wang and G.V. Eleftheriades, "Spatially shifted beam approach to sub-wavelength focusing", *Physical Review Letters*, 101, 113901, Sept. 12, 2008.

[2] A. M. H. Wong and G. V. Eleftheriades, "Adaptation of Schelkunoff's superdirective antenna theory for the realization of superoscillatory antenna arrays", *IEEE Antennas Wireless Propagat. Lett.*, vol. 9, pp. 315-318, Apr. 2010.

[3] L. Markley and G.V. Eleftheriades, "Two-dimensional subwavelength-focused imaging using a near-field probe at a quarter-wavelength working distance", *Journal of Applied Physics*, 107, 093102, May 04, 2010.

[4] L. Markley and G.V. Eleftheriades, "Detecting buried objects with subwavelength resolution using a near-field array probe", *IEEE Intl. Microwave Symposium*, Baltimore, MD, June 5-10, 2011.

[5] Ferreira, P. J. S. G. and A. Kempf, "Superoscillations: faster than the Nyquist rate," *IEEE Trans. Signal Process*, vol. 54, pp. 3732-3740, Oct. 2006.

[6] F. M. Huang, N. Zheludev, Y. Chen and De Abajo, F. J. G., "Focusing of light by a nanohole array," Appl. Phys. Lett., vol. 90, pp. 091119, Feb. 2007.

[7] F. M. Huang and N. I. Zheludev, "Super-resolution without evanescent waves," Nano Lett., vol. 9, pp. 1249-1254, Jan. 2009.

[8] A. M. H. Wong and G. V. Eleftheriades, "Sub-wavelength focusing at the multi-wavelength range using superoscillations: an experimental demonstration," *IEEE Trans. Antennas Propagat.*, vol. 59, pp. 4766-4776, Dec. 2011.

[9] A. M. H. Wong and G. V. Eleftheriades, "Temporal pulse compression beyond the Fourier transform limit," *IEEE Trans. Microwave Theory Tech.*, vol. 59, pp. 2173-2179, Sep. 2011.

[10] A.M.H. Wong and G.V. Eleftheriades, "Superoscillatory radar imaging: Improving radar range resolution beyond fundamental bandwidth limitations", *IEEE Microwave and Wireless Component Letters*, vol. 22, no. 3, pp. 147-149, March 2012.